

Article

Hypercoordinating Stannanes with *C,N*-Donor Ligands: A Structural, Computational, and Polymerization Study

Gloria M. D'Amaral ¹, Desiree N. Bender ¹, Nicola Piccolo ¹, Alan J. Lough ², Robert A. Gossage ¹ , Daniel A. Foucher ^{1,*} and R. Stephen Wylie ^{1,*}

¹ Department of Chemistry and Biology, Toronto Metropolitan University, 350 Victoria Street, Toronto, ON M5B 2K3, Canada; gloria.damaral@torontomu.ca (G.M.D.); desiree.bender@torontomu.ca (D.N.B.); nicola.piccolo@torontomu.ca (N.P.); gossage@torontomu.ca (R.A.G.)

² X-ray Laboratory, Department of Chemistry, University of Toronto, Toronto, ON M5H 3H6, Canada; alough@chemutoronto.ca

* Correspondence: daniel.foucher@torontomu.ca (D.A.F.); swylie@torontomu.ca (R.S.W.)

Abstract: Select triphenyl stannanes bearing either a formally sp^2 or sp^3 hybridized amine, *viz* 2-(pyC_2H_4) $SnPh_3$ (**2**: py = pyridinyl), 4-(pyC_2H_4) $SnPh_3$ (**3**), 2-(pzC_2H_4) $SnPh_3$ (**4**: pz = pyrazyl), and $Me_2N(CH_2)_3SnPh_3$ (**6**), were prepared and characterized by NMR spectroscopy (^{119}Sn , ^{13}C , 1H), and additionally, in the case of **2**, by single crystal X-ray diffraction. Bromination of **2** to yield 2-(pyC_2H_4) $SnPhBr_2$ (**8**) was achieved in good yield. X-ray crystallographic analysis of **8** revealed two unique molecules with 5-coordinate Sn centers featuring Sn-N distances of 2.382 (**5**) and 2.363 (**5**) Å, respectively. The calculated structures of the non- and hypercoordinating *C,N*-stannanes (**1–9**) were in good agreement with available crystallographic data. The relative stabilities of hyper- and non-hypercoordinating conformers obtained from conformational sampling were determined by comparison with reference conformers and by natural bond orbital (NBO) energetic analyses. Reduction of **8** to the dihydride species, 2-(pyC_2H_4) $SnPhH_2$ (**9**), and subsequent conversion to the polystannane, $[-2-(pyC_2H_4)SnPh]_n-$ (**15**), by transition metal-catalyzed dehydropolymerization was also achieved. Evidence for the decomposition of **15** into a redistributed distannoxane, $\{2-(pyC_2H_4)SnPh_2\}_2O$ (**16**), was also observed.

Keywords: hypercoordinate bonding; pyridyl stannanes; polystannanes



Citation: D'Amaral, G.M.; Bender, D.N.; Piccolo, N.; Lough, A.J.; Gossage, R.A.; Foucher, D.A.; Wylie, R.S. Hypercoordinating Stannanes with *C,N*-Donor Ligands: A Structural, Computational, and Polymerization Study. *Inorganics* **2024**, *12*, 122. <https://doi.org/10.3390/inorganics12040122>

Academic Editors: Francis Verpoort, Axel Klein and Shuang Xiao

Received: 2 April 2024
Revised: 15 April 2024
Accepted: 16 April 2024
Published: 18 April 2024



Copyright: © 2024 by the authors. Licensee MDPI, Basel, Switzerland. This article is an open access article distributed under the terms and conditions of the Creative Commons Attribution (CC BY) license (<https://creativecommons.org/licenses/by/4.0/>).

1. Introduction

The impact of hypercoordinate interactions between intramolecular donor ligands and Lewis acidic Sn centers in polystannanes, monomeric precursors, and related tin compounds has been a primary focus of our previous publications. These interactions, in which a pseudotetrahedral Sn center has distorted into an approximately trigonal bipyramidal geometry to accommodate a fifth ligand, are an example of a more general class of “hypervalent” molecules that has been described with various bonding formalisms [1]. An early proposal involved the extension of the covalent two-center two-electron bond concept to allow for three-center four-electron (3c-4e) interactions, the theoretical basis of which has been well established in the work by Musher [2], Pimentel [3], Rundle [4], and others [5,6]. 3c-4e interactions are important in a wide variety of *p*-block compounds and may be classified into several categories according to the number of electrons contributed by each of the three atom centers [7]. Dräger and co-workers have characterized the Sn hypercoordinate 3c-4e interaction as an intramolecular nucleophilic attack of the axial donor atom by lone pair donation into a σ^* orbital of the Sn center and the *trans*-ligand bonding atom (X), as reflected in the characteristically elongated tin–ligand bond [8]. A more recent formulation describes Group 14 element interactions with Lewis bases as “tetrel bonding” in a manner analogous to hydrogen bonding [9,10]. The Lewis acidic Sn is viewed as a σ -hole donor, with the σ -hole representing a region of positive electrostatic potential associated with

the Sn-X σ^* orbital. A more electron-withdrawing X atom contributes to a larger positive charge of the σ -hole donor, strengthening the association with the base acceptor. Both 3c-4e and tetrel σ -hole descriptions are consistent with non-covalent bonding of substantial ionic/electrostatic character. This was supported in a recent computational study of a dimer with Sn-O hypercoordinate/tetrel bonding that found that these interactions are mostly electrostatic in origin with little evidence of covalency [11]. In this context, we explored the additional significance of coordination interactions between Lewis acid Sn centers and Lewis basic C,N-donor ligands through structural modeling (Figure 1). We also investigated a new C,N-containing polystannane bearing a 2-pyridyl functionality that displays (by ^{119}Sn NMR) either metal-bound or metal-free N-atoms situated along the polymer backbone.

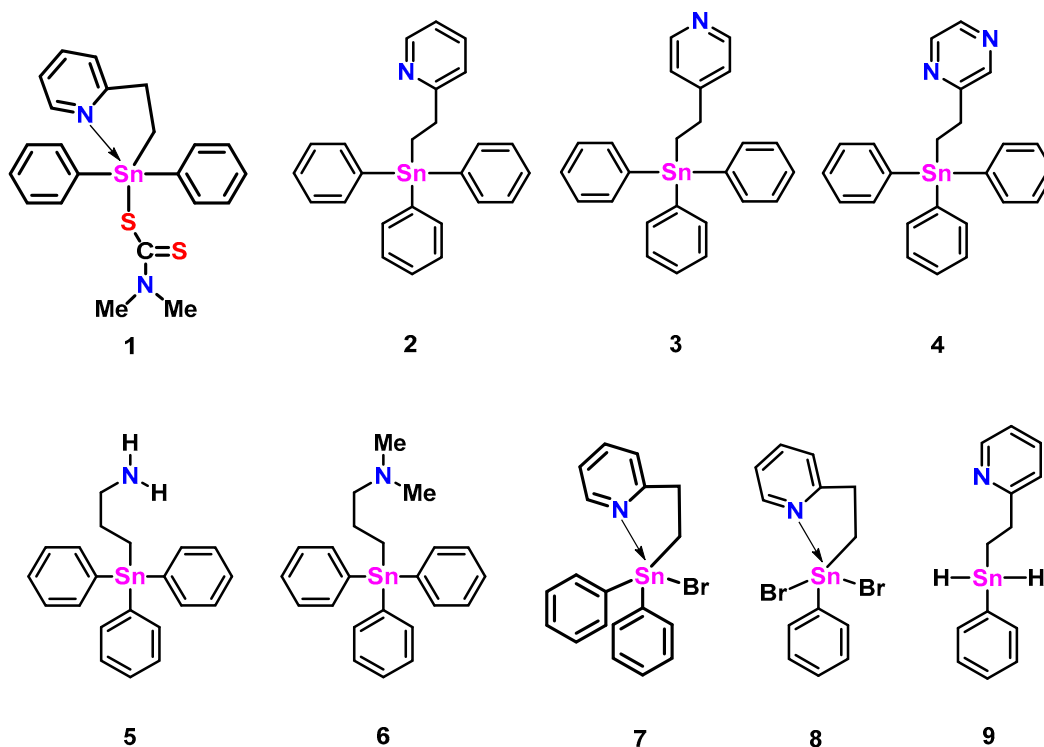


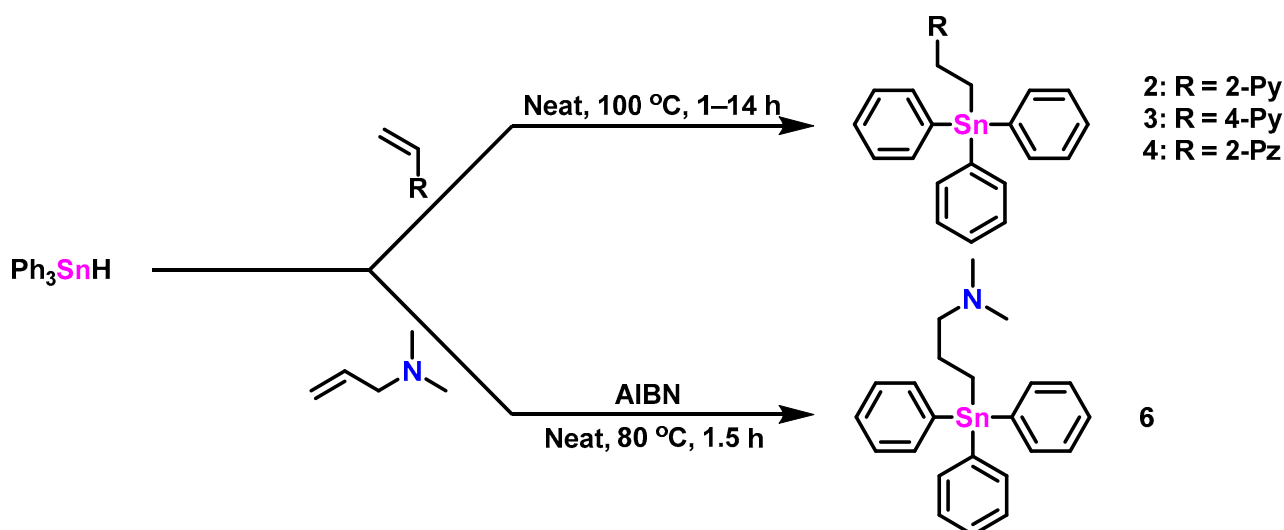
Figure 1. The various C,N-stannanes that are investigated herein.

2. Results

2.1. Triphenylstannanes

Compounds **2** and **3** were synthesized according to Molloy et al. [12] using a catalyst-free hydrostannylation reaction between Ph_3SnH and a molar excess of either 2- or 4-vinyl pyridine at $100\text{ }^\circ\text{C}$ for 1–2 h (Scheme 1). The products were recovered after recrystallization as white (**2**) and yellow (**3**) colored powders in modest yields (**2**: 76%, **3**: 59%). The NMR (^1H , ^{13}C) analysis of these species was in good agreement with the reported literature [12]. A comparatively longer (14 h, Scheme 1) hydrostannylation reaction between Ph_3SnH and a molar excess of 2-vinyl pyrazine at $100\text{ }^\circ\text{C}$ produced, after purification, a brown-colored gel of **4** in low yield (32%). Compound **5** was previously prepared by the Uhlig group by deprotection of an aminopropyltin compound using acid hydrolysis and is included in this study for structural and NMR data comparisons [13]. Compound **6**, previously prepared by Dräger et al. using the Grignard reaction of $\text{Me}_2\text{N}(\text{CH}_2)_3\text{MgCl}$ and Ph_3SnCl in 70% yield [8], was synthesized alternatively using an AIBN-assisted hydrostannylation reaction of Ph_3SnH and a stoichiometric amount of *N,N*-dimethylprop-2-en-1-amine ($80\text{ }^\circ\text{C}$ for 1.5 h; Scheme 1). The purified, translucent, yellow-colored gel of **6** was obtained in 75% yield. The ^1H and ^{13}C NMR (CDCl_3) spectral data for **6** were in agreement with the literature values [8]. The ^{119}Sn NMR resonances for compounds **3–5** (Table 1) found at ≈ -100 ppm

are typical of triphenylstannanes bearing a single alkyl substituent [14]. The ^{119}Sn NMR signal for **2** appears slightly more upfield (-108 ppm) and is suggestive of weak Sn-N hypercoordination present in solution.



Scheme 1. Reaction schemes for the synthesis of triphenylstannanes **2–4** and **6**.

A crystal of compound **2** suitable for single-crystal X-ray diffraction was obtained (Figure 2, left). The geometry around tin in **2** is distorted trigonal bipyramidal ($\tau_5 = 0.74$, where the τ_5 measure ranges from 1 for trigonal bipyramidal to 0 for square pyramidal geometries) [15] with equatorial bond angles between 102.38 (8°) and 120.81 (9°) and an axial bond angle (C20-Sn1-N1) of 165.14 (7°). The Sn1 and C20 bond length, located axially to the pyridyl nitrogen atom, is longer ($\approx 5\%$) than the other Sn carbon bonds of this molecule (see CCDC#2305421 files). The Sn-N distance in **2** is 2.888 (2) Å, slightly longer than that found with the rigid oxazoline **10** (Figure 3: Sn-N: 2.762 Å), but shorter than the more flexible methylene-bridged oxazoline **11** (Figure 3: Sn-N: 3.176 Å, 3.234 Å) [11]. Of note is that the less sterically hindered propyl amine structure of **5** (Figure 1) also possesses a relatively short Sn-N distance (2.740 (11) Å) [13].

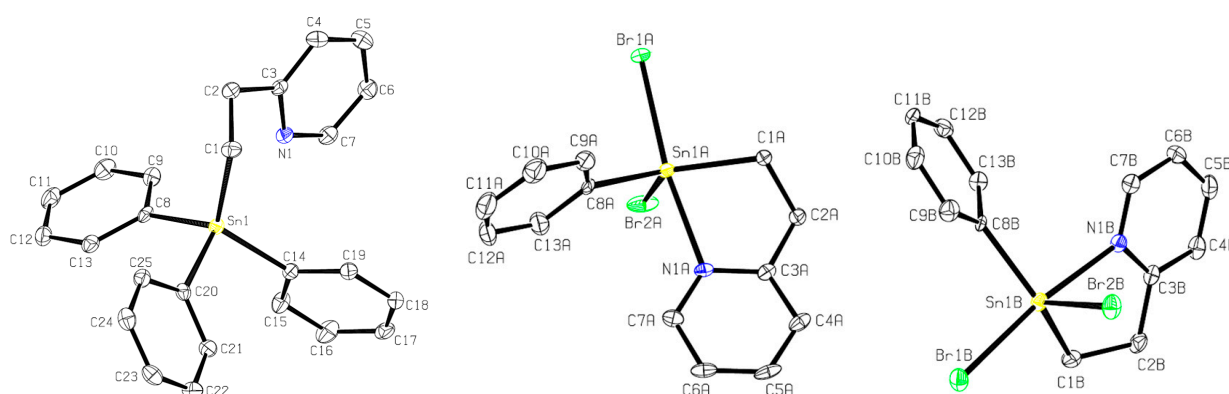


Figure 2. ORTEP representations of a unit cell molecule of **2** (left) and the two unique molecules of **8** (center and right) found in the unit cell. Thermal ellipsoids are drawn at the 30% level.

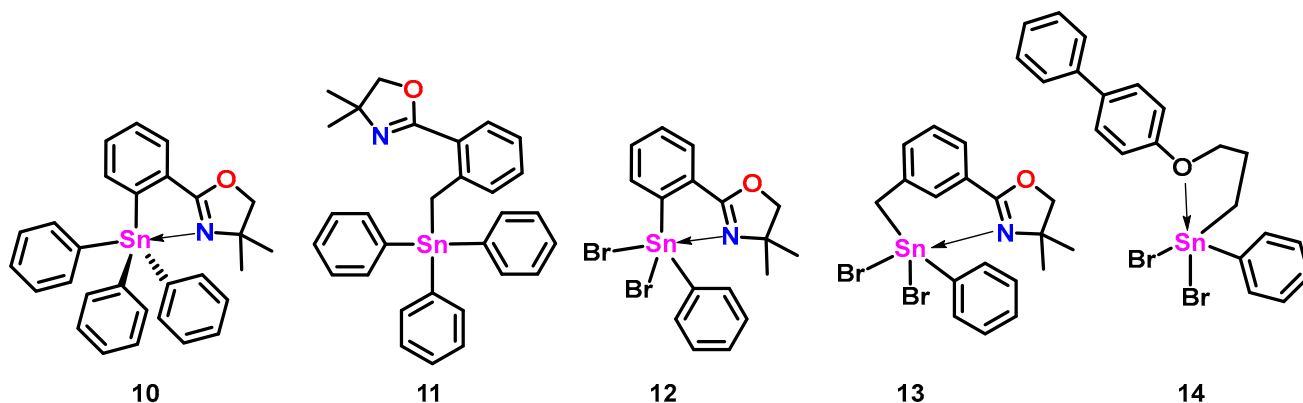
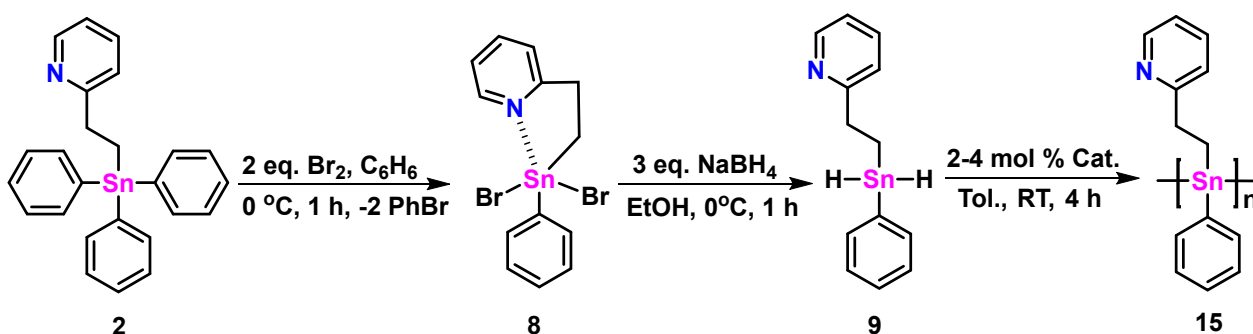


Figure 3. Previously structurally characterized stannanes.

2.2. Dihalo- and Dihydrido-Pyridyl Stannanes

The intermediate **8** was prepared using bromination of **2**, as shown in Scheme 2. After recrystallization, a white-colored solid was recovered with an 82% yield. The ^{119}Sn NMR resonance (CDCl_3) of **8** at -182.7 ppm is shifted >70 ppm upfield from **2**, and almost 40 ppm from **7** (Table 1), as reported by Molloy et al. [12].



Scheme 2. The synthetic pathway to transform **2** into polymeric **15**.

Table 1. Experimental and calculated Sn-N or Sn-O distances for stannanes 1–14 and corresponding observed ^{119}Sn NMR chemical shift values.

	^{119}Sn δ ppm (CDCl_3) ^a , (C_6D_6) ^b	Calc. Sn-N or Sn-O Distance (Å) ^c	Expt. Sn-N or Sn-O Distance (Å)
1	-202.0^a	2.56	2.486 (7) [12]
2	-108.3^a	2.94 (2.74 ^d)	2.888 (2)
3	-101.2^a	5.39	-
4	-104.3^b	3.34	-
5	-100.8^a	2.88	2.740 (11) [13]
6	-102.7^a	3.04	-
7	-143.5^a [12]	2.57 (2.52 ^d)	-
8	-183.9^a	2.50 (2.43 ^d)	2.382 (5), 2.363 (5)
9	-221.6^b	2.87	-
10	-157.1^a	2.73 ^d	2.762 (1) [16]
11	-126.0^a	2.96 ^d	3.176 (4), 3.234 (1) [16]
12	-290.6^a	2.41 ^d	2.383 (3) [16]
13	-248.2^a	2.49 ^d	2.424 (2) [16]
14	-53.3^a	-	2.918 (7) [14]

^a CDCl_3 . ^b C_6D_6 . ^c r²SCAN-3c, except where noted; lowest energy conformers. ^d M05-2X-GD3/LANL08d (Sn, Br); 6-31+G (d,p).

By comparison, the ^{119}Sn NMR resonance of **8** is significantly downfield of the signals observed for oxazoline-containing dibromides (e.g., **12**: ^{119}Sn $\delta = -290.6$ ppm, **13**: ^{119}Sn

$\delta = -248.2$ ppm), which may reflect the increased Lewis basic character of these ligands with Sn centers in solution [16]. Evidence of 5-coordinate geometries in **8**, **12**, and **13** in solution is also inferred from the ^{119}Sn NMR resonance for **14** (Table 1: ^{119}Sn $\delta = -53.3$ ppm) [14], which displays 5-coordinate geometry at Sn in the solid state but is likely 4-coordinate in solution.

A single crystal X-ray diffraction of **8** (Figure 2, center, right) revealed two unique molecules within the unit cell (see CCDC#2305460 files). The geometry around the tin center of these molecules is distorted trigonal bipyramidal ($\tau_5 = 0.56$ and $\tau_5 = 0.59$, respectively, for molecules *A* and *B*). Equatorial angles around the tin center range between 76.7 (2°) and 136.9 (2°). The Sn-N bond distances of both molecules of **8** (≈ 2.37 Å) are considerably shorter than the triphenyl analogue **2** (Table 1) and 5% shorter than the ethyl pyridyl diphenylstannane **1** bearing a tethered dithiocarbamate ligand (Figure 1; Table 1) [12]. Compound **9** was synthesized by a hydrogenation reaction using three equivalents of NaBH_4 in EtOH (1 h at 0°C ; Scheme 2) and isolated as a viscous, white-colored, translucent gel in low yield (33%). The ^1H NMR (C_6D_6) spectrum (Figure S26) of **9** reveals a singlet resonance at 5.90 ppm indicative of the two hydride atoms bound to Sn; this signal displays characteristic $^{117/119}\text{Sn}$ satellites ($^1J_{117\text{Sn}-1\text{H}} = 1766$, $^1J_{119\text{Sn}-1\text{H}} = 1848$ Hz) similar to other reported tin dihydrides [16–19]. The ^{119}Sn NMR (C_6D_6) spectrum (Figure S28) shows a single resonance, as predicted, at -221.6 ppm [16–19].

2.3. Computational Studies

In previous studies, we compared 28 X-ray crystallographic structures of hypercoordinate Sn compounds with density functional theory (DFT)-calculated structures to assess which levels of theory provided the best structural predictions based on a measure of the extent to which atomic coordinates coincided [16,20,21]. The PBE0-GD3BJ method generally provided the best overall prediction of molecular geometries, with M05-2X-GD3 also performing well. In the current study, structural comparisons of **2** and both crystallographic forms of **8** produced similar results (Table S1). However, calculated Sn-heteroatom distances in hypercoordinate stannanes are significantly model-dependent. For example, calculated gas phase Sn-N distances for the **8-A** conformer range from 2.43 Å (M05-2X-GD3) to 2.50 Å ($r^2\text{SCAN-3c}$) for a selection of model theories (Table S2). Application of a solvent model (Gaussian CPCM, CHCl_3 , Bondi radii, $\alpha = 1.2$) significantly shortens the calculated Sn-N distance for the **8-A** conformer from 2.49 Å to 2.38 Å (M06-GD3) and from 2.44 Å to 2.35 Å (PBE0-GD3BJ). However, increasing the electrostatic scaling factor α , as may be appropriate for some non-aqueous solvents [22,23], increases the calculated Sn-N distance. For $\alpha = 1.6$ in the previous solvent model, Sn-N distances are 2.42 Å (M06-GD3) and 2.38 Å (PBE0-GD3BJ), i.e., about 0.04 Å larger.

The calculation of solution NMR chemical shifts offers a possible benchmark comparison with experimental data to evaluate which level of theory/solution model most accurately predicts hypercoordinate distances in solution. Relativistic DFT calculations of ^{119}Sn NMR chemical shifts were previously carried out by others and us for several series of non-hypercoordinate reference compounds [21,24–26] and for four propylmethoxystannanes [21], with Boltzmann averaging of multiple conformers in some cases. The correlation between experimental and calculated ^{119}Sn NMR chemical shifts is very good for the non-hypercoordinate compounds, as noted in the above studies. The correlation is fairly insensitive to the level of theory used to calculate the structures of the compounds, probably because determining the chemical shifts relative to tetramethylstannane substantially corrects for theory-dependent differences in calculated structures.

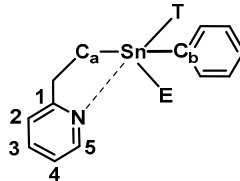
The calculated ^{119}Sn NMR chemical shifts for propylmethoxystannane conformers depend on the distance between the Sn center and the hypercoordinating O atom. Extended (non-hypercoordinate) conformers have predicted experimental shifts in excellent agreement with the non-hypercoordinating Sn compound linear correlation. For hypercoordinated stannanes, the agreement is less satisfactory. While structures calculated for gas phase propylmethoxystannane conformers provide Boltzmann-averaged chemical shifts in good agreement with the linear correlation, the introduction of a solvent model lowers the

calculated chemical shifts by 5–25 ppm [21]. The greater differences are observed for the more strongly hypercoordinating compounds. Some hypercoordinate N-donor compounds in the current study (2, 7, 9) showed similar underestimates (16–23 ppm), even when used with a model selected for longer Sn-N distances (M06-GD3, CHCl₃ model, Bondi radii, $\alpha = 1.6$). The agreement is worse for models that predict shorter hypercoordinate bond distances.

One possible explanation is that condensed phase calculations underestimate hypercoordinate bond distances by overestimating the extent of hypercoordination. However, even with models that predict the longest hypercoordinate distances, we have been unable to calculate satisfactory ¹¹⁹Sn NMR chemical shifts for compounds with hypercoordinate donors. A second possibility is that 5-coordination around the Sn center leads to a systematic error in the relativistic DFT chemical shift calculations as compared to 4-coordinate compounds. Determining this requires hypercoordinate reference compounds with limited conformational variation; we are currently actively investigating such a system.

Insights into the structural and energetic aspects of hypercoordination can be gained from conformational searches of a related set of compounds, such as the *C,N*-stannanes in this study (Figure 1). The CREST program [27] from the Grimme group was used for conformational sampling, and the resulting ensembles were refined by DFT calculations using the efficient and accurate r²SCAN-3c method [28]. Major conformers, Gibbs energies, and Boltzmann-weighted contributions are presented in Table S3. A number of non-hypercoordinate conformations are stabilized by phenyl ring π -stacking with the pyridyl (2-B–2-F, 3-A–3-C, 9-A, 9-E) or pyrazine ring (4-A–4-C, 4-E, 4-F) substituents. Multiple hypercoordinate conformers for a given compound result from dihedral rotations of Sn phenyl substituents, as seen in conformers 5-A–5-D and 6A–6C, for example. Hypercoordinate conformers show characteristic lengthening of the Sn bond to the ligand atom *trans*- to the hypercoordinate N atom, with the extent of lengthening dependent on the identity of the ligand atom: Sn-Br, ~0.04–0.06 Å; Sn-C(Ph), ~0.01–0.02 Å; Sn-H, ~0.02 Å. For steric reasons, 3 has no hypercoordinate conformers. Compound 4 has one (4-D), which accounts for approximately 12% of conformers; it resembles 2-A but with a slightly longer (0.01 Å) Sn-N distance. The average Sn-N distance in 6-A–6-C is about 0.19 Å longer than in 5-A–5-D, consistent with steric hindrance due to the amine methyl groups in 6. Compounds 1 and 7–9 each have two hypercoordinate forms, one with a *trans*-S, Br, or H atom and one with a *trans*-C(Ph) atom. In each case, the contribution of the *trans*-C(Ph) conformer is minor in comparison to the other hypercoordinate conformers of the compound.

The strength of hypercoordinate interactions can be assessed by comparison to non-hypercoordinate reference compounds. Table 2 shows the relative Gibbs energy differences between the most stable conformers (1-A–9-A) and reference conformers in which the pyridyl or amine alkyl linkage is fully extended in an *anti*-conformation with the Sn substituent. The reference conformation minimizes strain and steric interactions in the alkyl linkage for a stable, non-hypercoordinate conformation. Non-hypercoordinate conformers (3-A, 4-A, and 9-A) are 7–13 kJ mol⁻¹ more stable than their extended reference conformers due to π interactions between phenyl and pyridyl or pyrazyl rings. Strongly hypercoordinate conformers with *trans*-Br substituents (7-A, 8-A) are stabilized by ~38 kJ mol⁻¹. Conformers with *trans*-H or Ph substituents (2-A, 5-A, 6-A, 9-B) are much weaker with stabilizations of ~10–12 kJ mol⁻¹, about the same as the inter-ring interactions noted in the non-hypercoordinate conformers. *Trans*-Ph conformers of 7 and 8 (7-C, 8-E), which are much less stable than the *trans*-Br conformers, are stabilized by ~18 kJ mol⁻¹. This larger stabilization (as compared to 2-A, 5-A, and 6-A) probably reflects the influence of the equatorial Br substituent(s) on the Lewis acidity of the Sn center.

Table 2. Relative Gibbs energies and NBO interaction energies for selected conformers of stannanes 1–9.


Conformer	G_{ref}^{a-} $G_{conf}/\text{kJ mol}^{-1}$	Sn-N dist./Å	NBO N Lone Pair Donor Anti-Bond Acceptor Interaction Energy/ kJ mol^{-1}					
			Sn-T ^b	Sn-C ^a	Sn-C ^b	Sn-E ^c	C ₁ -C ₂	C ₄ -C ₅
1-A	28.2	2.56	79.1	28.7	19.3	13.8	41.1	35.0
2-A	15.6	2.94	18.2	9.5	7.8	4.8	44.6	38.2
3-A	7.0	5.39	^d	^d	^d	^d	41.2	41.8
4-A	12.6	3.34	3.4	^d	^d	^d	41.0	38.4
5-A	10.3	2.88	22.9	11.5	9.9	8.5	-	-
6-A	10.9	3.04	12.6	7.5	5.8	3.8	-	-
7-A	37.9	2.58	80.1	26.7	19.5	13.7	41.2	35.7
8-A	37.3	2.50	86.2	36.6	27.3	21.3	40.3	34.0
9-A	11.2	3.15	5.9	2.5	^d	2.3	46.4	40.0
9-B	10.8	2.87	19.2	10.0	9.0	7.3	44.2	37.9

^a Reference conformers have fully extended alkyl linkages with pyridyl or amine and an Sn substituent in an *anti*-conformation. For examples, see Conformers 3-ref and 5-ref in Table S3. ^b T = -S(SCSNMe₂): 1-A; -C(Ph): 2-A, 3-A, 4-A, 5-A, 6-A; -Br: 7-A, 8-A; -H: 9-A, 9-B. ^c E = -C(Ph): 1-A, 2-A, 3-A, 4-A, 5-A, 6-A, 7-A; -Br: 8-A; -H: 9-A, 9-B. ^d <2.0 kJ mol⁻¹.

A natural bond orbital (NBO) energetic analysis [29] provides an alternative measure of the strength of hypercoordinate interactions without the need for reference conformations. Table 2 presents selected second-order perturbative estimates of donor–acceptor (N lone pair anti-bond) interactions on an NBO basis. These represent corrections required to reconcile the idealized Lewis structure description with the calculated molecular wavefunction. For example, N lone pair donations to the C₁–C₂ and C₄–C₅ anti-bonds reflect the participation of N electron density in pyridyl ring resonance that is unrepresented in the idealized Lewis structure. The interaction energy of the N lone pair with the anti-bond between Sn and the atom *trans*- to it (Sn–T*) reflects the increased stabilization due to the hypercoordination absent in the Lewis structure, as does the lengthened Sn bond to the *trans*-ligand atom. There is a significant energy difference between the strongly hypercoordinate 1-A, 7-A, and 8-A (79–86 kJ mol⁻¹) and the more weakly hypercoordinate 2-A, 5-A, 6-A, and 9-B (12–22 kJ mol⁻¹). Unlike the relative conformer energies considered previously, the N lone pair Sn–T* interaction energies for the non-hypercoordinate conformers (3-A, 4-A, and 9-A) are clearly distinguished from the weakly hypercoordinate ones. Finally, it is notable that the N lone pair anti-bond interaction energies with the other Sn substituent atoms are larger for the strongly hypercoordinate 1-A, 7-A, and 8-A. This probably reflects increased ionic character in the Sn-substituent bonds of the Lewis structure to account for greater electrostatic stabilization in the molecular wavefunction.

2.4. Synthesis of Polymer 15, Characterization, and Stability

Polymer 15 was prepared using a dehydrocoupling polymerization reaction of monomer 9 using a 4 mol% catalytic loading of Wilkinson’s catalyst (Scheme 2). The polymerization occurred over a 4 h time period at RT to yield an orange-colored gel after solvent removal. The crude product was purified by standard methods and recovered as a yellow-colored powder with a 56% yield. The synthesis of 15 was also executed using half the loading (2 mol%) of catalyst, which resulted in the recovery, after purification, of a yellow-colored polymer solid in an improved 73% yield.

¹¹⁹Sn NMR (C₆D₆) analysis of polymer 15 prepared with 4 mol% of catalyst (Figure 4) reveals the appearance of two Sn environments in what may be described as an “open” and “closed” conformation ($\delta = -132$ and -173 ppm, respectively). Hypercoordinate interac-

tions of ≈ 30 – 40% of the nitrogen atoms of the pyridyl moiety with the proximate Sn centers resulted in an upfield chemical shift (≈ 40 ppm) relative to the 4-coordinate Sn centers. Similar behavior has been previously observed in other polystannanes bearing secondary potential metal-binding ligand groups [16,19,21,30]. To confirm that both resonances are indeed a result of an “open” and “closed” confirmation around the Sn center, a few drops of d^8 -THF were added to the NMR sample, as previously demonstrated by Pau et al. for other hypercoordinate polystannanes [30]. The coordination of THF to the Sn center displaces the hypercoordinate ligand and results in a single “open” ^{119}Sn signal at $\delta = -132$ ppm (Figure S34).

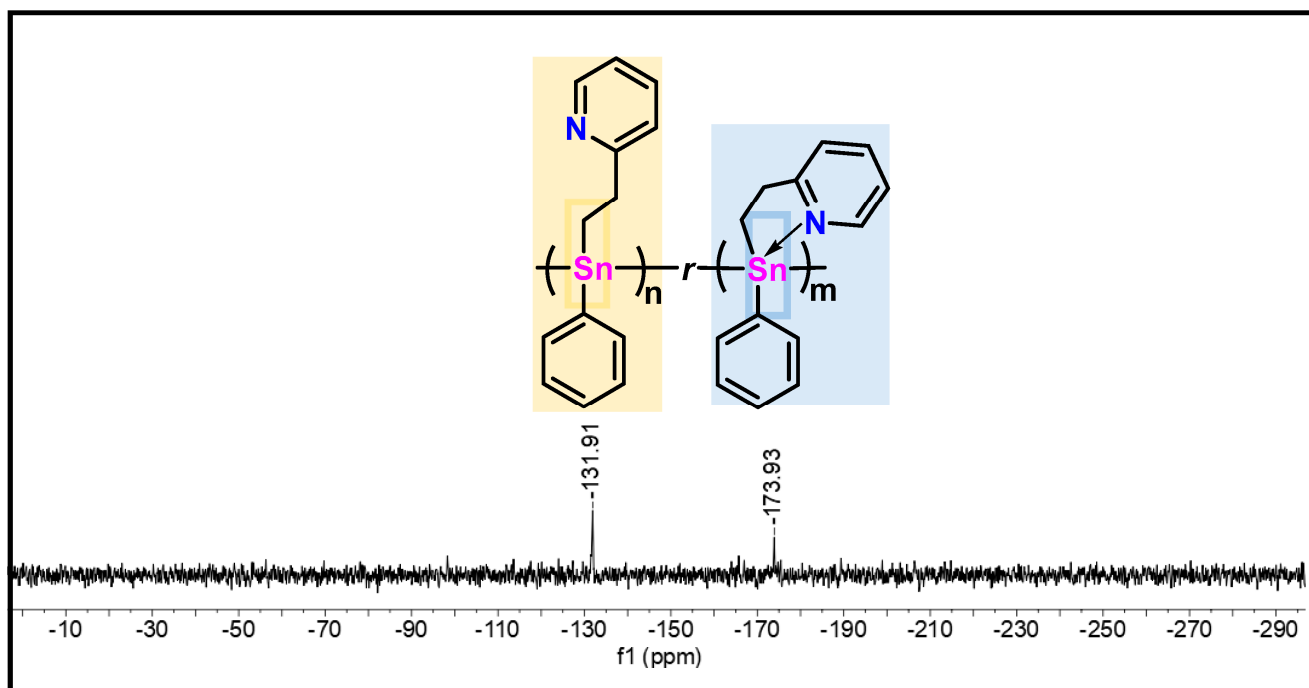


Figure 4. ^{119}Sn NMR spectrum (C_6D_6) of polymer **15** prepared with 4 mol% cat.

A solid powder sample of **15** was left exposed to ambient conditions (21°C , relative humidity $\approx 65\%$, natural light) for 30 d to test its long-term stability. A ^{119}Sn NMR spectrum obtained after 30 d of exposure (Figure 5) was compared to the sample $t = 0$. A new, and as yet unassigned, signal at -167.2 ppm indicates that some degradation of **15** occurs in the solid state under these conditions. However, both the open and closed resonances attributed to polymer **15** are still present in significant concentration after this evaluation, which is a considerable improvement compared to 4-coordinate polystannanes, which typically degrade readily (<1 h) after exposure to similar conditions [31–33].

A molecular weight determination (GPC) for **15** prepared with a 4 mol% catalyst revealed a trimodal distribution. Analysis of the largest peak in the GPC indicates that it has a relatively low molecular weight (11,200 Da, $D = 2.90$, Figure 6). A more narrowly distributed, slightly higher molecular weight of polymer **15** was obtained using the 2 mol% catalyst loading ($M_w \approx 20,000$ Da, $D = 1.8$).

DSC analysis of the semi-crystalline polymer **15** prepared at a 2 mol% loading of catalyst (Figure 7) shows a weak, reversible T_g at 139.5°C and a stronger reversible melting temperature observed at 231.8°C .

Further confirmation of the polymer morphology of **15** was afforded by PXRD, which displays three broad d -spacings centered at $2\theta = 6.75$, 13.9 , and 16.7 (Figure 8), again consistent with semi-crystalline behavior for this polystannane.

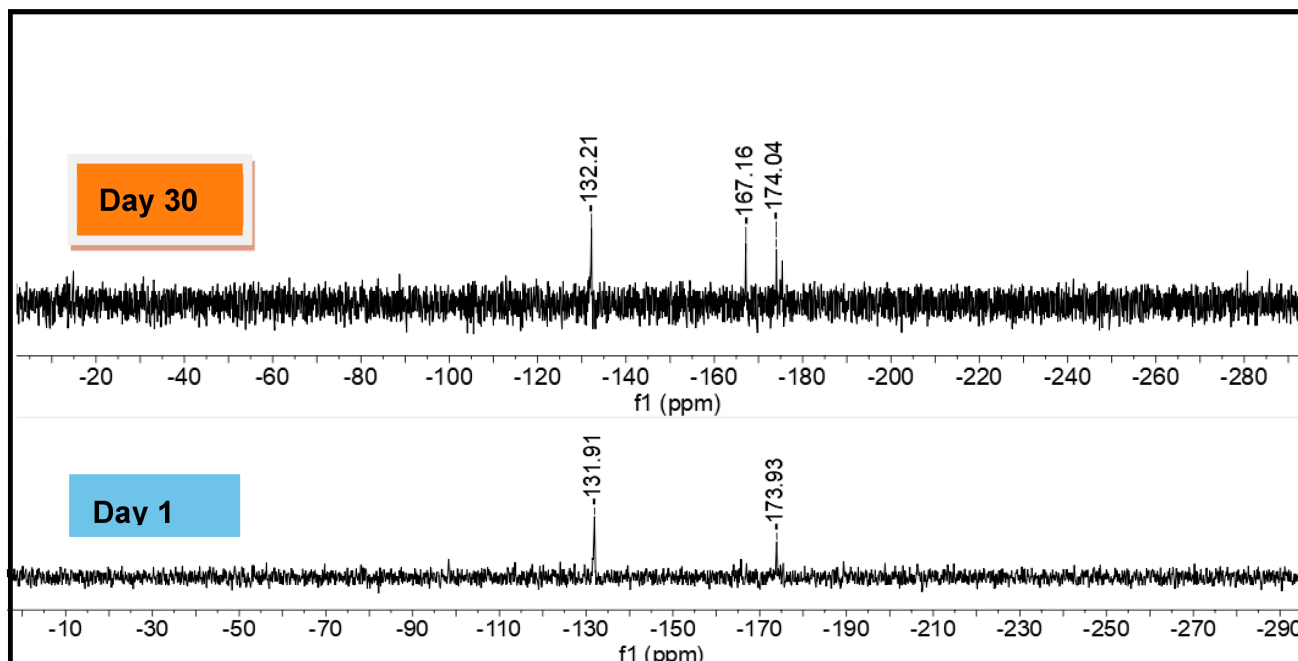


Figure 5. Comparison of ^{119}Sn NMR spectra (C_6D_6) of polymer 15 after 1 and 30 d.

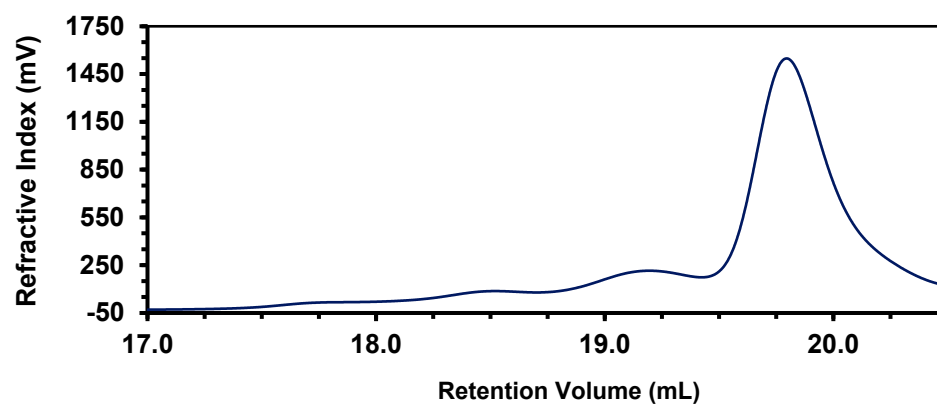


Figure 6. GPC trace (RI) of polymer 15.

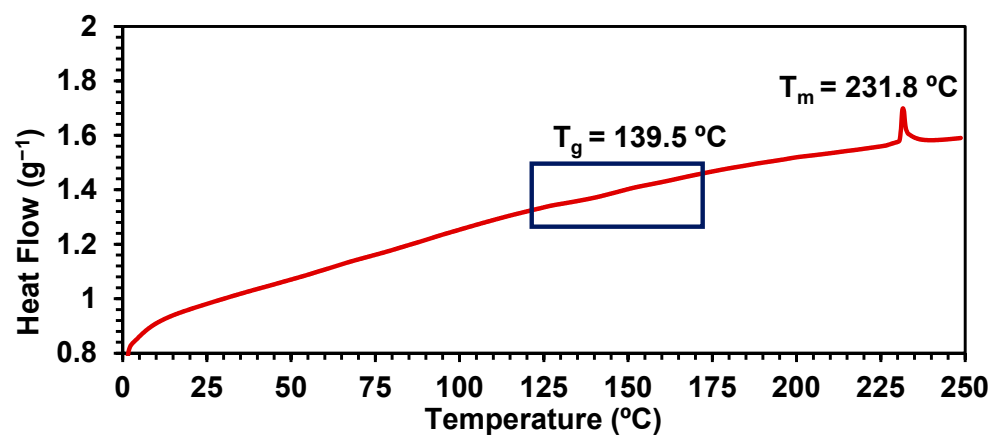


Figure 7. DSC thermogram of polymer 15.

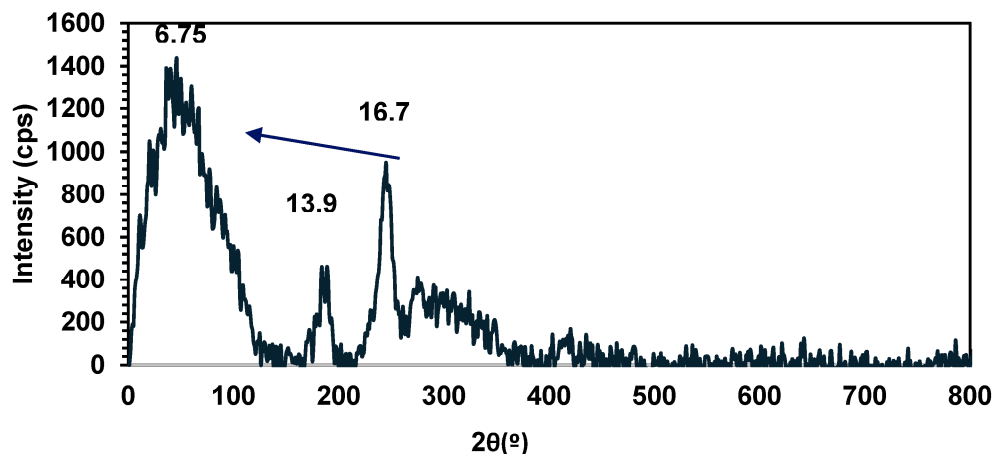


Figure 8. PXRD diffractogram of 15.

UV-Vis spectroscopy of a 0.01 M solution of 15 in THF did not exhibit a clear λ_{\max} , which could be attributable to the $\sigma\text{-}\sigma^*$ transition for polymers containing a conjugated backbone of Sn atoms. However, significant tailing between 300 and 450 nm was detected (Figure 9).

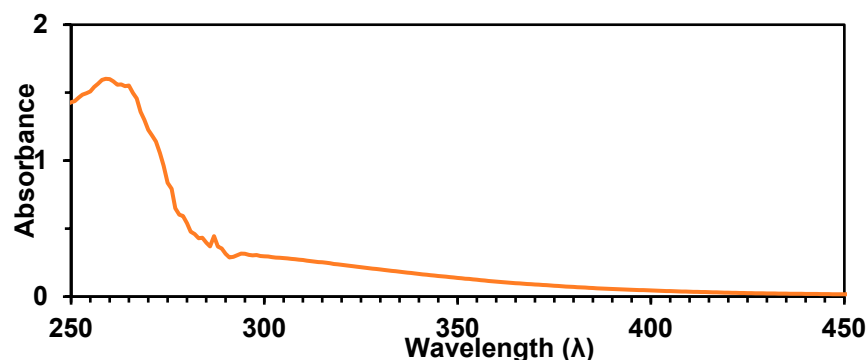


Figure 9. UV-Vis spectrum of homopolymer 15 in THF.

Similar results were previously reported for an asymmetric, flexible polystannane with an ether-linked biphenyl substituent [32].

2.5. Evidence of Redistribution and Distannoxane Formation from 15

Evidence of both redistribution reactions and distannoxane formation was observed in the course of carrying out additional polymerization attempts of 9 using similar catalyst loadings (2–4 mol% $\text{RhCl}(\text{PPh}_3)_3$). A ^{119}Sn NMR (C_6D_6) analysis of the crude mixture of one of these attempts revealed a major resonance at $\delta = -135.4$ ppm, near the previously assigned “open” conformer of 15 ($\delta = -132$ ppm), with no evidence for the “closed” conformer. Several other minor resonances ($\delta = 204$, -116 , -128.5 , and -184 ppm) were also detected; these may be attributed to smaller oligomers or to 5- or 6-membered Sn cyclic materials. Such compounds have been previously observed for other polystannanes [33].

Additional washings (3×) of this polymer sample were conducted by dissolving the crude product mixture in a minimal amount of toluene (1 mL) and precipitating the sample into an excess of stirring cold hexanes (20 mL). Further analysis of the recovered stannane materials by ^{119}Sn NMR (C_6D_6) spectroscopy displayed only two prominent resonances ($\delta = -135.9$ and -183.7 ppm: Figure S35). When a few drops of d^8 -THF were added to the NMR tube containing the purified sample (Figure S36), ^{119}Sn NMR analysis revealed a decrease in the intensity of the resonance of the open conformation of 15 and an increase in the intensity of the previously unassigned resonance at $\delta = -184.6$ ppm. After further purification steps, a ^1H NMR (C_6D_6) spectrum consistent with distannoxane 16

was detected. A single ^{119}Sn NMR (C_6D_6) resonance for **16** at $\delta = -183.8$ ppm is noted (Figure 10).

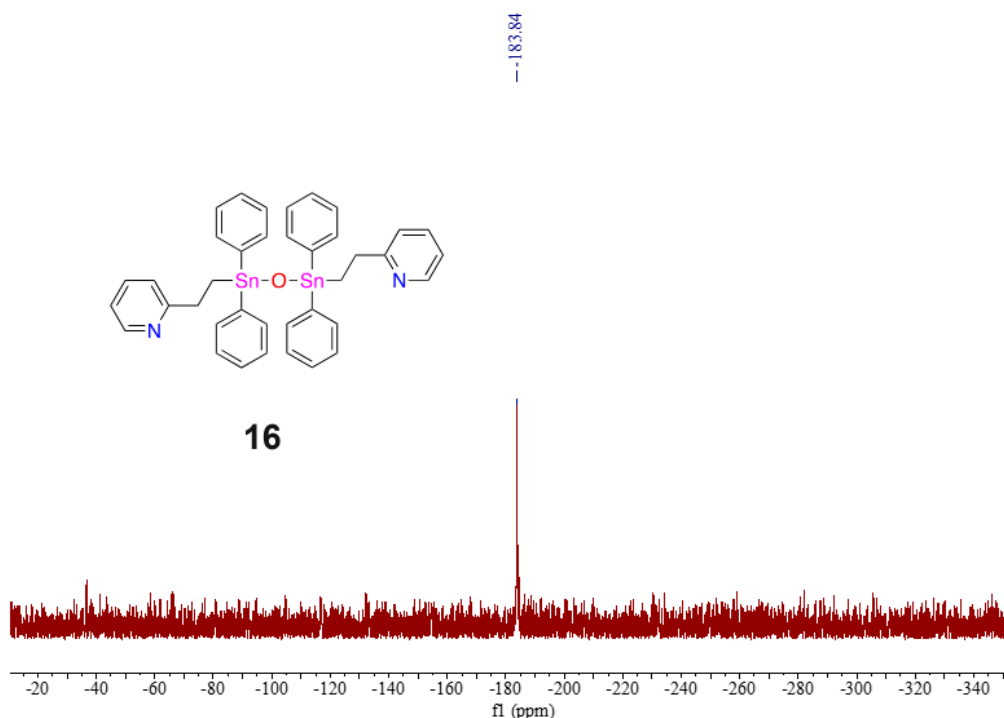


Figure 10. ^{119}Sn NMR spectrum (C_6D_6) of distannoxane **16**.

To confirm the chemical identity of **16**, direct analysis in real time (DART) mass spectrometry was performed, and a molecular ion for a protonated distannoxane was detected. The formation of **16** from the decomposition/re-distribution and oxidation reactions suggests that the Sn-Sn bonds of **15** are susceptible to reactivity in solution. Decomposition/re-distribution of the pyridyl polymer into distannoxane **16** occurs relatively quickly as a result of the purification process, even after rigorous Schlenk line techniques without air or light were followed. The proposed distannoxane **16** was recovered as a yellow-colored solid.

3. Materials and Methods

3.1. General Considerations

All reagents and solvents were obtained from Sigma-Aldrich (St. Louis, MO, USA) and used as received, unless otherwise indicated. Solvents were dried either through an MBraun solvent drying system (MBraun, Stratham, NH, USA) or through vacuum distillation and stored under an inert nitrogen atmosphere. All reactions were carried out under a nitrogen atmosphere using Schlenk techniques, unless otherwise noted. Nuclear magnetic resonance (NMR) spectroscopic experiments were carried out on a Bruker 400 MHz spectrometer (Bruker, Billerica, MA, USA) using CDCl_3 or C_6D_6 as the solvent. ^1H NMR (400 MHz) and ^{13}C NMR (100.6 MHz) spectra were referenced to the residual proton and central carbon resonance of the solvent. The ^{119}Sn NMR (149 MHz) was referenced to SnMe_4 as an external standard. All the chemical shifts are given in δ (ppm) relative to the solvent and assigned to atoms. All NMR spectra were analyzed on MestReNova v6.0.2 software (Mestrelab Research, Escondido, CA, USA). High-resolution mass spectrometry was performed using an accuTOF DART-MS at the University of Toronto. The molecular weights of polymers were determined by gel permeation chromatography (GPC) using a Viscotek Triple Model 302 Detector system (Malvern Panalytical, Malvern, UK) equipped with a Refractive Index Detector (RI), a four-capillary differential viscometer (VISC), and a right-angle (90°) laser light scattering detector. GPC columns were calibrated against polystyrene standards (American Polymer Standards Corp., Mentor, OH, USA). A

flow rate of 1.0 mL min⁻¹ was used with ACS-grade THF as eluent. GPC samples were prepared using 10–15 mg of polymers per mL of THF and filtered using a 0.45 µm filter. All reactions were carried out under a nitrogen atmosphere using Schlenk techniques, unless otherwise described.

3.2. Synthesis of 2-(pyC₂H₄)SnPh₃ (2)

Triphenyltin hydride (0.500 g, 1.42 mmol) and 2-vinylpyridine (0.23 mL, 2.14 mmol) were added into a 50 mL dry Schlenk flask attached with a reflux condenser and heated to 100 °C for 2 h. The solution was allowed to cool. The crude solid was recrystallized from petroleum ether (b.p. 60–95 °C) and gravity filtered. The mother liquor was removed under reduced pressure, and the remaining solid was again recrystallized from 1:1 MeOH:Et₂O to yield a white-colored powder. The NMR data (¹H, ¹³C) match the reported literature data within experimental error [12]. Yield: 0.496 g, 76%. m.p. 78 °C. ¹H NMR (400 MHz, CDCl₃, δ): 8.26 (d, ³J = 4.8 Hz, 1H, H_a), 7.55–7.53 (m, 6H, H_i), 7.51–7.47 (m, 1H, H_c), 7.34–7.33 (m, 9H, H_j, H_k), 7.08t (d, ³J = 7.8 Hz, 1H, H_d), 7.00 (t, 1H, H_b), 3.24 (t, ³J = 7.8 Hz, 2H, H_g), 1.88 (t, ³J = 7.8 Hz, 2H, H_f) ppm. ¹³C {¹H} NMR (100 MHz, CDCl₃, δ): 162.92 (C_e), 148.80 (C_a), 140.38 (C_i), 137.06 (C_j), 136.27 (C_c), 128.49 (C_l), 128.27 (C_k), 122.45 (C_d), 121.12 (C_b), 34.03 (C_f), 10.58 (C_g) ppm. ¹¹⁹Sn {¹H} NMR (149 MHz, CDCl₃, δ): –108.3 ppm.

3.3. Synthesis of 4-(pyC₂H₄)SnPh₃ (3)

Triphenyltin hydride (8.01 g, 22.8 mmol) and 4-vinylpyridine (3.70 mL, 34.2 mmol) were added into a dry Schlenk flask attached with a reflux condenser and placed into a pre-heated oil bath at 100 °C for 1.5 h. The solution was allowed to cool, and MeOH (20 mL) was added, whereby the impurity, Ph₃SnSnPh₃, precipitated. After gravity filtration, the solution was evaporated under reduced pressure, and the remaining yellow gel was recrystallized using heptane to yield a white-colored powder. The NMR data (¹H, ¹³C) match the reported literature data within experimental error [12]. Yield: 6.13 g, 59%. m.p. 99 °C. ¹H NMR (400 MHz, CDCl₃, δ): 8.43 (d, ³J = 5.94 Hz, 2H, H_a), 7.51 (m, 6H, H_g), 7.39–7.38 (m, 9H, H_h&H_i), 7.08 (d, ³J = 6.04 Hz, 2H, H_b), 2.97 (t, ³J = 5.54 Hz, 2H, H_d), 1.79 (t, ³J = 8.57 Hz, 2H, H_e) ppm. ¹³C {¹H} NMR (100 MHz, CDCl₃, δ): 153.48 (C_c), 149.75 (C_a), 138.11 (C_f), 136.96 (C_g), 129.10 (C_i), 128.64 (C_h), 123.29 (C_b), 31.86 (C_d), 11.33 (C_e) ppm. ¹¹⁹Sn {¹H} NMR (149 MHz, CDCl₃, δ): –101.2 ppm. HRMS-DART (*m/z*) = 458.0952 (M+H) calculated for C₂₅H₂₄NSn; found 458.09252.

3.4. Synthesis of 2-(pzC₂H₄)SnPh₃ (4)

Triphenyltin hydride (0.5 g, 1.42 mmol) and 4-vinylpyridine (0.29 mL, 2.90 mmol) were added into a dry Schlenk flask attached with a reflux condenser and placed into a pre-heated oil bath at 100 °C for 14 h. The solution was allowed to cool, and MeOH (20 mL) was added, whereby the impurity, Ph₃SnSnPh₃, precipitated. After gravity filtration, the solution was evaporated under reduced pressure, and a brown semi-solid was recovered. The brown-colored gel was dissolved in a minimal amount of THF (1–2 mL) and precipitated into a flask of cold, stirring hexanes. After the solution was allowed to settle, the liquid was decanted. A brown-colored gel was recovered after evaporation under reduced pressure. The semi-solid was heated to 90 °C under static vacuum to remove remaining traces of 2-vinyl pyrazine and yield a brown-colored gel. Yield: 0.21 g, 32%. ¹H NMR (400 MHz, C₆D₆, δ): 8.00 (s, 1H, H_a), 7.87 (d, ³J = 2.4 Hz, 1H, H_c), 7.76 (t, ³J = 1.6 Hz, 1H, H_b), 7.53 (m, 6H, H_h), 7.17 (m, 9H, H_i&H_j), 2.86 (t, ³J = 7.5 Hz, 2H, H_e), 1.64 (t, ³J = 7.5 Hz, 2H, H_f) ppm. ¹³C {¹H} NMR (100 MHz, C₆D₆, δ): 144.44 (C_c), 143.11 (C_a), 142.2 (C_b), 137.03 (C_d), 128.59 (C_{ij}), 128.38 (C_j), 30.82 (C_e), 9.94 (C_f) ppm. ¹¹⁹Sn {¹H} NMR (149 MHz, C₆D₆, δ): –104.3 ppm. HRMS-DART (*m/z*) = 459.0905 (M+H) calculated for C₂₄H₂₃N₂Sn; found 459.0882.

3.5. Synthesis of $\text{Me}_2\text{N}(\text{CH}_2)_3\text{SnPh}_3$ (**6**)

Compound **5** was prepared by adding Ph_3SnH (0.75 g, 2.14 mmol) to a dry 50 mL Schlenk flask, along with 3 mol% of AIBN and *N,N*-dimethylprop-2-en-1-amine (1.27 mL, 10.7 mmol). The flask was placed in a pre-heated oil bath at 80 °C and allowed to react for 1.5 h. The crude product was dissolved in MeOH, whereby a small amount (5–7%) of the impurity $\text{Ph}_3\text{SnSnPh}_3$ precipitated and was subsequently removed by gravity filtration. The solvent was evaporated, and the crude product was sublimed at 70 °C to collect additional impurities on the cold finger, leaving a pure light yellow-colored gel in the chamber. The NMR data (^1H , ^{13}C) match the reported literature data within experimental error [8]. Yield: 75% (0.705 g). ^1H NMR (400 MHz, CDCl_3 , δ): 7.65 (m, 6H, H_f), 7.43 (m, 9H, H_g & H_h), 2.37 (t, $^3J = 7.12$ Hz, 2H, H_b), 2.19 (s, 6H, H_a), 1.97 (quint, $^3J = 7.73$ Hz, 2H, H_c), 1.61 (t, $^3J = 8.4$ Hz, 2H, H_d) ppm. ^{13}C { ^1H } NMR (100 MHz, CDCl_3 , δ): 138.05 (C_e), 135.96 (C_f), 127.73 (C_h), 127.39 (C_g), 62.30 (C_b), 44.44 (C_a), 23.44 (C_c), 7.37 (C_d) ppm. ^{119}Sn { ^1H } NMR (149 MHz, CDCl_3 , δ): –100.77 ppm.

3.6. Synthesis of $2\text{-(pyC}_2\text{H}_4\text{)SnPhBr}_2$ (**8**)

A solution of **2** (0.500 g, 1.09 mmol) prepared with 10 mL of C_6H_6 was added to a 50 mL Schlenk flask and cooled to 0 °C. Br_2 (0.350 g, 2.19 mmol) was added dropwise, and the reaction mixture was stirred for 1 h. The solvent was removed under reduced pressure to yield a red-colored gel. The crude product was recrystallized from 9:1 petroleum ether (60–95 °C):ethyl acetate to yield the pure product as white-colored needles. Yield: 82% (0.415 g). m.p. 99 °C. ^1H NMR (400.13, CDCl_3 , δ): 8.15 (d, 1H, H_a , $^3J_{1\text{H}-1\text{H}} = 4.91$ Hz), 7.86 (ddd, 1H, H_c , $^3J_{1\text{H}-1\text{H}} = 7.68$ Hz, $^4J_{1\text{H}-1\text{H}} = 1.58$ Hz), 7.64–7.62 (m, 2H, H_i), 7.42–7.39 (m, 4H, H_j , H_k , H_d), 7.31–7.28 (m, 1H, H_b), 3.47 (t, 2H, H_g , $^3J_{1\text{H}-1\text{H}} = 7.30$ Hz), 2.22 (t, 2H, H_f , $^3J_{1\text{H}-1\text{H}} = 7.30$ Hz) ppm. ^{13}C { ^1H } NMR (100.61 MHz, CDCl_3 , δ): 158.37 (C_e), 145.90 (C_a), 142.23 (C_h), 139.81 (C_c), 134.69 (C_i), 130.26 (C_k), 128.91 (C_a), 124.82 (C_d), 123.49 (C_b), 30.69 (C_f), 21.68 (C_g) ppm. ^{119}Sn { ^1H } NMR (149.21 MHz, CDCl_3 , δ): –183.92 ppm. HRMS-DART (m/z): [M-Br] calculated for $^{12}\text{C}_{13}^{1}\text{H}_{13}^{79}\text{Br}_1^{14}\text{N}_1^{119}\text{Sn}_1$: 381.92534; found 381.92478.

3.7. Synthesis of $2\text{-(pyC}_2\text{H}_4\text{)SnPhH}_2$ (**9**)

A solution of **8** (0.50 g, 1.08 mmol) in EtOH (10 mL) was added to a solution of NaBH_4 (0.12 g, 3.20 mmol) in EtOH (10 mL) in a 100 mL Schlenk flask at 0 °C. After 1 h, hexanes (20 mL) were added to the reaction mixture and subsequently quenched with degassed H_2O (12 mL). The organic layer was separated and washed with degassed H_2O (3 × 30 mL), dried with MgSO_4 , and filtered. The solvent was removed under reduced pressure to obtain a colorless, translucent gel of **9**. Yield: 33% (0.11 g). ^1H NMR (400 MHz, C_6D_6 , δ): 8.29 (d, $^3J = 4.4$ Hz, 1H, H_a), 7.65–7.60 (m, 2H, H_i), 7.23–7.11 (m, 3H, H_j & H_k), 6.93 (td, 1H, $^3J = 7.6$, 1.8 Hz, 1H, H_d), 6.52 (m, 2H, H_b & H_c), 5.90 (s, $^{117}\text{Sn}-^{119}\text{Sn}J = 1766.1$ Hz, $^{119}\text{Sn}-^{119}\text{Sn}J = 1848.1$ Hz, 2H, H_l), 2.91 (t, $^3J = 7.1$ Hz, 2H, H_g), 1.40 (t, $^3J = 7.1$ Hz, 2H, H_f) ppm. ^{13}C { ^1H } NMR (100 MHz, C_6D_6 , δ): 162.13 (C_e), 147.99 (C_a), 139.53 (C_h), 137.42 (C_i), 135.68 (C_d), 128.15–128.12 (C_j & C_k), 122.34 (C_l), 120.93 (C_b), 33.95 (C_f), 8.14 (C_g) ppm. ^{119}Sn { ^1H } NMR (149 MHz, C_6D_6 , δ): –221.6 ppm. Note: Several attempts were made to acquire the HRMS for this compound, but its hydrolytic and thermal instability complicated analysis.

3.8. Synthesis of Polymer **15** Prepared with 2 mol% Wilkinson Catalyst

Wilkinson's catalyst, $\text{RhCl}(\text{PPh}_3)_3$ (0.049 g, 0.053 mmol), was dissolved in 5 mL of dry toluene, added to a foil-wrapped 100 mL Schlenk flask, and allowed to stir at RT for 10 min to ensure activation. A solution of **9** (0.40 g, 1.31 mmol) in toluene (5 mL) was added to the catalyst solution, and the reaction was allowed to stir at RT for 4 hr. The solvent was removed in vacuo, and the crude product was dissolved in a minimal amount of THF and transferred dropwise to a 100 mL flask containing a stirring solution of cold hexanes. A yellow-colored precipitate formed immediately, and the solution was stirred for an additional 5 min and allowed to settle. The hexane layer was decanted and the

residual solvent removed in vacuo to obtain a dry yellow-colored powder of **15**. Yield: 56% (0.34 g). $M_w = 11,200$ Da. $D = 2.90$. ^1H NMR (400 MHz, C_6D_6 , δ): 7.94 (m, 1H, H_a), 7.85 (m, 5H, H_i & H_j & H_k), 7.07 (m, 3H, H_b & H_c & H_d), 2.90 (m, 2H, H_g), 1.32 (m, 2H, H_f) ppm. ^{119}Sn NMR (149 MHz, C_6D_6 , δ): -173.9 , -131.9 ppm. Please note: Several attempts at carrying out traditional elemental analysis were unsuccessful. We attribute this to the overall moisture and possible light sensitivity of this polystannane in contrast to other hypercoordinate polystannanes.

3.9. Synthesis of Polymer **15** Prepared with 4 mol% Wilkinson Catalyst

Wilkinson's catalyst, $\text{RhCl}(\text{PPh}_3)_3$ (0.01g, 0.011 mmol), dissolved in 5 mL of dry toluene, was added to a foil-wrapped 100 mL Schlenk flask and allowed to stir at RT for 10 min to ensure activation. A solution of **9** (0.17 g, 0.56 mmol) in toluene (5 mL) was added to the catalyst solution, and the reaction was allowed to stir at RT for 4 hr. The solvent was removed in vacuo, and the crude product was dissolved in a minimal amount of THF and transferred dropwise to a 100 mL flask containing a stirring solution of cold hexanes. A yellow-colored precipitate formed immediately, and the solution was stirred for an additional 5 min and allowed to settle. The hexane layer was decanted and the residual solvent removed in vacuo to obtain a dry yellow-colored powder of **15**. Yield = 73% (0.12 g). ^{119}Sn NMR (149 MHz, C_6D_6 , δ): -132.3 ppm.

3.10. Isolation of Pyridyl Distannoxane **16**

During the purification and analysis of 0.5 g of **15**, decomposition of the Sn-Sn bond and redistribution of the phenyl ligands were observed, leading to the formation of a yellow-colored distannoxane **16**. Yield: 32% (0.15 g). ^1H NMR (400 MHz, C_6D_6 , δ): 7.87–7.85 (m, 6H), 7.78–7.71 (m, 6H), 7.60–7.59 (d, 2H), 6.71–6.66 (m, 2H), 6.31–6.29 (d, 2H), 6.16–6.13 (t, 2H), 2.85–2.81 (t, 4H, H_f), 1.93–1.89 (t, 4H, H_g) ppm; $^{119}\text{Sn}\{^1\text{H}\}$ NMR (149 MHz, C_6D_6 , δ): -183.84 ppm. HRMS-DART (m/z) = 777.09443 (M+H) calculated for $^{12}\text{C}_{38}^{1}\text{H}_{36}^{14}\text{N}_2^{16}\text{O}^{119}\text{Sn}_2$; found 777.09549.

3.11. Computational Details

Cartesian coordinates for experimental structures were extracted from crystallographic information files (.cif) with OpenBabelGUI [34]. All geometric optimizations and frequency calculations were carried out using either the Gaussian 16 suite of programs (G16 Rev C.01) [35] or ORCA (5.0.4) [36]. Gaussian calculations used PBE0 "PBE1PBE" [37], M05-2X [38], and B3-PW91 [39] DFT functionals with Grimme's D3 empirical dispersion function and, for PBE0 and B3-PW91, Becke-Johnson damping [40]. The LANL08d basis set was used for Sn, with the 6-31+G (d,p) basis set used for all other atoms. Tight convergence criteria and superfine integration grids were used for all geometry optimizations. Solvation was implemented with the default Gaussian 16 method (the Polarizable Continuum Model using the integral equation formalism variant (IEF-PCM)) with Bondi radii and adjusted values of the electrostatic scaling factor α (1.1–1.6) [41]. ORCA calculations used the $r^2\text{SCAN-3c}$ composite method, which incorporates a modified def2-mTZVPP basis set and the $r^2\text{SCAN}$ meta-GGA [28] with D4 dispersion [42,43] and geometrical counterpoise corrections [44]. Tight convergence criteria ("verytightscf" and "verytightopt") were used in combination with the DEF-GRID 3 integration grid. All geometric optimizations with Gaussian and ORCA software were verified to be potential energy minima by frequency calculations. The CREST program [27] was used for conformational sampling, and the resulting ensembles were refined by $r^2\text{SCAN-3c}$ geometric optimization. Conformer fractions for compounds were calculated by determining $q_i = \alpha e^{-\Delta G/\text{RT}}$ for each conformer i , where α is the total degeneracy of the conformer. Dividing q_i by the sum of all q gives the fraction of conformer i . Natural bond orbital (NBO) analysis used the NBO 7.0 program in combination with $r^2\text{SCAN-3c}$ single-point energy calculations [45].

4. Conclusions

Intramolecular hypercoordination in stannane compounds has been well-characterized in solid-state studies. Although DFT computational methods give broadly similar results, the Sn-N separation distances for the *C,N*-stannanes in this study are sensitive to the specific method used. The selection of an optimal approach for solvated complexes and accurately calculating ^{119}Sn chemical shifts remains challenging. Conformational and energetic analyses of compounds **1–9** provided measures of the relative strength of some hypercoordinate interactions. Evidence for the formation of polymer **15**, as well as other side products, was isolated from the transition-metal-catalyzed dehydropolymerization of dihydride compound **9**. The initial analysis of **15** by ^{119}Sn NMR (C_6D_6) spectroscopy displayed two resonances for both closed and open polymer confirmations along the polymer at high catalyst loading and a single resonance consistent with an open conformation at lower catalyst loading [21,30]. Further purification and analysis of polymer **15** resulted in the isolation of the redistributed distannoxane **16**, confirmed by HRMS. This strongly suggests that the Sn-Sn bond strength in polymer **15** containing the flexible pyridyl ligand is not as strong as previously believed. The purification and analysis of **15** likely resulted in exposure to moisture, cleaving it and leading to **16**. This is in contrast to previous work with polystannanes bearing an oxazoline substituent or polystannanes with a flexible pendant oxygen donor. Investigation of other *C,N*-containing monomers and polymers with more rigid backbones is ongoing.

Supplementary Materials: The following supporting information can be downloaded at: <https://www.mdpi.com/article/10.3390/inorganics12040122/s1>, NMR spectra (^1H , ^{13}C , ^{119}Sn , and 2D NMR) in Figures S1–S38, and computational data in Tables S1–S3. Crystallographic data for compounds **2** (CCDC#2305421) and **8** (CCDC#2305460) were deposited with the Cambridge Crystallographic Data Base. The CIF and checkCIF output files are included.

Author Contributions: G.M.D., D.N.B. and N.P. carried out the experimental research work; D.A.F. led the research project; D.A.F., R.A.G. and R.S.W. drafted the manuscript; A.J.L. was the crystallographer for all the structures in this manuscript; R.S.W. carried out the computational calculations. All authors have read and agreed to the published version of the manuscript.

Funding: This work was supported by the NSERC Discovery Grant program (Natural and Engineering Science Research Council of Canada, App # RGPIN-2022-03771).

Data Availability Statement: The original contributions presented in the study are included in the article, further inquiries can be directed to the corresponding author.

Acknowledgments: The computational studies for R. Stephen Wylie were made possible by the Digital Research Alliance of Canada and the Toronto Metropolitan Analytical Facility.

Conflicts of Interest: The authors declare no conflicts of interest.

References

1. Norman, N.C.; Pringle, P.G. Hypervalence: A Useful Concept or One That Should Be Gracefully Retired? *Chemistry* **2022**, *4*, 1226–1249. [CrossRef]
2. Musher, J.I. The Chemistry of Hypervalent Molecules. *Angew. Chem. Int. Ed.* **1969**, *8*, 54–68. [CrossRef]
3. Pimentel, G.C. The Bonding of Trihalide and Bifluoride Ions by the Molecular Orbital Method. *J. Chem. Phys.* **1951**, *19*, 446–448. [CrossRef]
4. Hach, R.J.; Rundle, R.E. The Structure of Tetramethylammonium Pentafluoride. *J. Am. Chem. Soc.* **1951**, *73*, 4321–4324. [CrossRef]
5. Reed, A.E.; Schleyer, P.V.R. Chemical Bonding in Hypervalent Molecules. The Dominance of Ionic Bonding and Negative Hyperconjugation over d-Orbital Participation. *J. Am. Chem. Soc.* **1990**, *112*, 1434–1445. [CrossRef]
6. Kutzelnigg, W. Chemical Bonding in Higher Main Group Elements. *Angew. Chem. Int. Ed.* **1984**, *23*, 272–295. [CrossRef]
7. Green, M.L.H.; Parkin, G. The classification and representation of main group element compounds that feature three-center four-electron interactions. *Dalton Trans.* **2016**, *45*, 18784–18795. [CrossRef]
8. Zickgraf, A.; Beuter, M.; Kolb, U.; Dräger, M.; Tozer, R.; Dakternieks, D.; Jurkschat, K. Nucleophilic Attack within Ge, Sn and Pb Complexes Containing $\text{Me}_2\text{N}(\text{CH}_2)_3$ - As a Potential Intramolecular Donor Ligand. *Inorg. Chim. Acta* **1998**, *275–276*, 203–214. [CrossRef]
9. Scheiner, S. Origins and properties of the tetrel bond. *Phys. Chem. Chem. Phys.* **2021**, *23*, 5702–5717. [CrossRef]

10. Bauzá, A.; Seth, S.K.; Frontera, A. Tetrel bonding interactions at work: Impact on tin and lead coordination compounds. *Coord. Chem. Rev.* **2019**, *384*, 107–125. [CrossRef]
11. Ullah, H.; Twamley, B.; Waseem, A.; Rauf, M.K.; Tahir, M.N.; Platts, J.A.; Baker, R.J. Tin···Oxygen Tetrel Bonding: A Combined Structural, Spectroscopic, and Computational Study. *Cryst. Growth Des.* **2017**, *17*, 4021–4027. [CrossRef]
12. Mahon, M.F.; Molloy, K.C.; Waterfield, P.C. Synthesis, Characterization, and Reaction Chemistry of [2-(2-Pyridyl)Ethyl]-, [2-(4-Pyridyl)Ethyl]-, and [2-(2-Oxo-4-Pyrrolidiny)Ethyl]Triphenyltin(IV). *Organometallics* **1993**, *12*, 769–774. [CrossRef]
13. Pichler, J.; Torvisco, A.; Bottke, P.; Wilkening, M.; Uhlig, F. Novel Amino Propyl Substituted Organo Tin Compounds. *Can. J. Chem.* **2014**, *92*, 565–573. [CrossRef]
14. Deacon, P.R.; Devylder, N.; Hill, M.S.; Mahon, M.F.; Molloy, K.C.; Price, G.J. Organotin Compounds Bearing Mesogenic Sidechains: Synthesis, X-Ray Structures and Polymerisation Chemistry. *J. Organomet. Chem.* **2003**, *687*, 46–56. [CrossRef]
15. Addison, A.W.; Rao, T.N.; Reedijk, J.; van Rijn, J.; Verschoor, G.C. Synthesis, Structure, and Spectroscopic Properties of Copper(II) Compounds Containing Nitrogen-Sulphur Donor Ligands; the Crystal and Molecular Structure of Aqua[1,7-Bis(N-Methylbenzimidazol-2'-yl)-2,6-Dithiaheptane]Copper(II) Perchlorate. *J. Chem. Soc. Dalton Trans.* **1984**, *7*, 1349–1356. [CrossRef]
16. Bender, D.N.; Lough, A.J.; Wylie, R.S.; Gossage, R.A.; Foucher, D.A. Preparation and DFT Studies of κ^2C,N -Hypercoordinated Oxazoline Organotins: Monomer Constructs for Stable Polystannanes. *Inorganics* **2020**, *8*, 35. [CrossRef]
17. Komsta, Z.; Cmoch, P.; Stalinski, K. Intramolecularly Sn-N Coordinated Organotin Hydrides. *Pol. J. Chem.* **2006**, *80*, 1259–1292. [CrossRef]
18. Matkowska, D.; Gola, M.; Śniezek, M.; Cmoch, P.; Staliński, K. Structural Assignment of Organotin Hydrides Containing the Oxazoline Ligand. *J. Organomet. Chem.* **2007**, *692*, 2036–2045. [CrossRef]
19. Pau, J.; D'Amaral, G.M.; Lough, A.J.; Wylie, R.S.; Foucher, D.A. Synthesis and Characterization of Readily Modified Poly(Aryl)(Alkoxy)Stannanes by Use of Hypercoordinated Sn Monomers. *Chem. Eur. J.* **2018**, *24*, 18762–18771. [CrossRef]
20. Khan, A.; Pau, J.; Loungxay, J.; Magobenny, T.; Wylie, R.S.; Lough, A.J.; Foucher, D.J. Hypercoordinated organotin(IV) compounds containing C,O- and C,N- chelating ligands: Synthesis, characterisation, DFT studies and polymerization behaviour. *Organomet. Chem.* **2019**, *900*, 120910. [CrossRef]
21. Pau, J.; Choi, J.-W.; Silverthorne, K.; Ranne, M.; Wylie, R.S.; Gossage, R.A.; Lough, A.J.; Foucher, D.A. New Hypercoordinating Organostannanes for the Modular Functionalization of Mono- and Polystannanes: Synthetic and Computational Studies. *Eur. J. Inorg. Chem.* **2022**, *2022*, e202100937. [CrossRef]
22. Luque, F.J.; Zhang, Y.; Alemán, C.; Bachs, M.; Gao, J.; Orozco, M. Solvent Effects in Chloroform Solution: Parametrization of the MST/SCRF Continuum Model. *J. Phys. Chem.* **1996**, *100*, 4269–4276. [CrossRef]
23. Xu, L.; Coote, M.L. Improving the Accuracy of PCM-UAHF and PCM-UAKS Calculations Using Optimized Electrostatic Scaling Factors. *J. Chem. Theory Comput.* **2019**, *15*, 6958–6967, Correction in *J. Chem. Theory Comput.* **2020**, *16*, 816–817. [CrossRef] [PubMed]
24. Bagno, A.; Casella, G.; Saielli, G. Relativistic DFT Calculation of ^{119}Sn Chemical Shifts and Coupling Constants in Tin Compounds. *J. Chem. Theory Comput.* **2006**, *2*, 37–46. [CrossRef] [PubMed]
25. Sindlinger, C.P.; Aicher, F.S.W.; Weseman, L. Cationic Stannylenes: In Situ Generation and NMR Spectroscopic Characterization. *Inorg. Chem.* **2017**, *56*, 548–560. [CrossRef] [PubMed]
26. Stückrath, J.B.; Gasevic, T.; Bursch, M.; Grimme, S. Benchmark Study on the Calculation of ^{119}Sn NMR Chemical Shifts. *Inorg. Chem.* **2022**, *61*, 3903–3917. [CrossRef] [PubMed]
27. Pracht, P.; Bohle, F.; Grimme, S. Automated exploration of the low-energy chemical space with fast quantum chemical methods. *Phys. Chem. Chem. Phys.* **2020**, *22*, 7169–7192. [CrossRef] [PubMed]
28. Grimme, S.; Hansen, A.; Ehlert, S.; Mewes, J.-M. r²SCAN-3c: A “Swiss army knife” composite electronic-structure method. *J. Chem. Phys.* **2021**, *154*, 064103. [CrossRef]
29. Weinhold, F. Natural Bond Orbital Analysis: A Critical Overview of Relationships to Alternative Bonding Perspectives. *J. Comput. Chem.* **2012**, *33*, 2363–2379. [CrossRef]
30. Pau, J.; Lough, A.J.; Wylie, R.S.; Gossage, R.A.; Foucher, D.A. Proof of Concept Studies Directed Towards Designed Molecular Wires: Property Driven Synthesis of Air and Moisture-Stable Polystannanes. *Chem. Eur. J.* **2017**, *57*, 14367–14374. [CrossRef]
31. Trummer, M.; Choffat, F.; Smith, P.; Caseri, W. Polystannanes: Synthesis, Properties, and Outlook. *Macromol. Rapid. Commun.* **2012**, *33*, 448–460. [CrossRef]
32. Khan, A.; Komejan, S.; Patel, A.; Lombardi, C.; Lough, A.J.; Foucher, D.A. Reduction of C,O-Chelated Organotin(IV) Dichlorides and Dihydrides Leading to Protected Polystannanes. *J. Organomet. Chem.* **2015**, *776*, 180–191. [CrossRef]
33. Imori, T.; Lu, V.; Cai, H.; Tilley, T.D. Metal-Catalyzed Dehydropolymerization of Secondary Stannanes to High Molecular Weight Polystannanes. *J. Am. Chem. Soc.* **1995**, *117*, 9931–9940. [CrossRef]
34. O'Boyle, N.M.; Banck, M.; James, C.A.; Morley, C.; Vandermeersch, T.; Hutchison, G.R. Open Babel: An open chemical toolbox. *J. Cheminf.* **2011**, *3*, 33. [CrossRef]
35. Gaussian Release 2016: Gaussian 16, Rev. C 01; Gaussian Inc.: Wallingford, CT, USA, 2016; Available online: <https://gaussian.com/citation> (accessed on 1 April 2024).
36. Neese, F. Software update: The ORCA program system—Version 5.0. *WIREs Comput. Mol. Sci.* **2022**, *12*, e1606. [CrossRef]
37. Perdew, J.P.; Burke, K.; Ernzerhof, M. Generalized gradient approximation made simple. *Phys. Rev. Lett.* **1996**, *77*, 3865–3868. [CrossRef] [PubMed]

38. Zhao, Y.; Schultz, N.E.; Truhlar, D.G. Design of Density Functionals by Combining the Method of Constraining Satisfaction with Parametrization for Thermochemistry. *J. Chem. Theory Comput.* **2006**, *2*, 364–382. [[CrossRef](#)]
39. Perdew, J.P. Unified Theory of Exchange and Correlation Beyond the Local Density Approximation. In *Electronic Structure of Solids '91*; Ziesche, P., Eschig, H., Eds.; Akademie Verlag: Berlin, Germany, 1991; pp. 11–20.
40. Grimme, S.; Ehrlich, S.; Goerigk, L. Effect of the Damping Function in Dispersion Corrected Density Functional Theory. *J. Comput. Chem.* **2011**, *32*, 1456–1465. [[CrossRef](#)]
41. Tomasi, J.; Mennucci, B.; Cammi, R. Quantum mechanical continuum solvation models. *Chem. Rev.* **2005**, *105*, 2999–3093. [[CrossRef](#)]
42. Caldeweyher, E.; Bannwarth, C.; Grimme, S. Extension of the D3 dispersion coefficient model. *J. Chem. Phys.* **2017**, *147*, 034112. [[CrossRef](#)] [[PubMed](#)]
43. Caldeweyher, E.; Ehlert, S.; Hansen, A.; Neugebauer, H.; Spicher, S.; Bannwarth, C.; Grimme, S. A generally applicable atomic-charge dependent London dispersion correction. *J. Chem. Phys.* **2019**, *150*, 154122. [[CrossRef](#)] [[PubMed](#)]
44. Kruse, H.; Grimme, S. A geometrical correction for the inter- and intra-molecular basis set superposition error in Hartree-Fock and density functional theory calculations for large systems. *J. Chem. Phys.* **2012**, *136*, 154101. [[CrossRef](#)] [[PubMed](#)]
45. Glendening, E.D.; Badenhop, J.K.; Reed, A.E.; Carpenter, J.E.; Bohmann, J.A.; Morales, C.M.; Karafiloglou, P.; Landis, C.R.; Weinhold, F. *NBO 7.0*; Theoretical Chemistry Institute, University of Wisconsin: Madison, WI, USA, 2018.

Disclaimer/Publisher's Note: The statements, opinions and data contained in all publications are solely those of the individual author(s) and contributor(s) and not of MDPI and/or the editor(s). MDPI and/or the editor(s) disclaim responsibility for any injury to people or property resulting from any ideas, methods, instructions or products referred to in the content.